Electron spin resonance of substitutional nitrogen in silicon

M. Belli

Laboratorio MDM, IMM-CNR, Via C. Olivetti, 2, 20864, Agrate Brianza (MB), Italy

M. Fanciulli[*]

Università degli Studi di Milano-Bicocca, Dipartimento di Scienza dei Materiali, Via R. Cozzi 53, 20126, Milano, Italy and
Laboratorio MDM, IMM-CNR, Via C. Olivetti, 2, 20864, Agrate Brianza (MB), Italy

D. Batani

University Bordeaux, CEA, CNRS, CELIA (Centre Laser Intense at Applications), UMR 5107, F-33405 Talence, France and
Università degli Studi di Milano-Bicocca, Dipartimento di Fisica, Piazza della Scienza 3, 20126, Milano, Italy

The development of silicon-based nanoscale technology for the realization of single electron, single spin quantum devices demands deep donor-based systems to achieve a major breakthrough in the field: high-temperature operation. Here, we suggest that, despite some preparation difficulties, substitutional nitrogen in silicon (N_{Si}) represents an interesting candidate for this purpose, being observable by electron paramagnetic resonance (EPR) at room temperature. We report a study of the nature and dynamics of substitutional nitrogen in silicon, the so-called SL5 paramagnetic center, by X-band continuous-wave EPR, complemented by pulsed EPR. Both natural and ^{28}Si isotopically enriched nitrogen-doped silicon samples have been used, the latter providing an improvement in the accuracy of the spin Hamiltonian parameters.

I. INTRODUCTION

Impurities in silicon have been proposed as one of the most promising systems for the implementation of spin-based single-atom devices [1]. The requirements for such a challenging application have already been met, at liquid helium temperatures, by shallow donors such as phosphorus in silicon, where the donor spins act as qubits controlled by electrical potentials and by irradiation with microwaves [1–8]. The long coherence time at low temperature allows efficient quantum error correction [9], especially in isotopically enriched spinless ^{28}Si. However, a major breakthrough in the field would be to prove similar functionalities in devices working at room temperature. This motivates the search for new Si-based systems with potential for operation at temperatures higher than 4.2 K. Deep donors [10] and double donors [11] in silicon have been considered as a possible solution of the problem since the freeze-out regime is maintained at higher temperatures compared to the shallow donors, and in such a state the electron wave function is relatively unaffected by external sources of decoherence. Bismuth, for example, has been recently investigated and coherence times compatible with fault-tolerant quantum information processing have been measured for temperatures up to 40 K [10,12–16].

The Si:N system has already been investigated extensively [17–24]. Continuous-wave electron paramagnetic resonance (EPR) allowed the determination of the microstructure and revealed peculiar dynamical properties [25–27]. Former investigations on nitrogen-doped silicon highlighted the difficulty in the preparation of the substitutional monoatomic impurity N_{Si} (the so-called SL5 center) and the presence of

a distortion along one of the four equivalent ⟨111⟩ directions, which yields an off-center displacement of the nitrogen atom leading to a reduction of the point symmetry from T_d to C_{3v}. There has been a debate on the possible origin of the distortion. The two most likely mechanisms have been identified either as a pseudo-Jahn-Teller distortion induced by the degeneracy of excited states [17] or chemical rebonding of hyperdeep states [19]. As a consequence of the distortion, the gyromagnetic factor and the hyperfine interaction become anisotropic. EPR investigations in K band evidenced that the donor orientation is frozen at low temperatures, but above ~120 K it was possible to observe the effects of thermally activated reorientational dynamics with an energy barrier of 110 ± 20 meV [26]. The analysis of paramagnetic resonance spectra at high temperatures well above the onset of the reorientation jumps allowed Murakami *et al*. [27] to point out that also a metastable on-center configuration with large hyperfine interaction, and an energy level located 73 meV above the fundamental state, takes part in the dynamics, though only indirect evidence of this fact could be obtained.

In this paper, we report continuous-wave (CW) EPR investigations of substitutional nitrogen in silicon (N_{Si}), which is observable by EPR up to room temperature and even above [27]. We focus on the EPR spectrum, on its temperature evolution, and on the different contributions to the linewidth. A thorough study of spin-spin and spin-lattice relaxation will be the subject of a following paper [28]. The investigation is complemented by a pulsed EPR study of the instantaneous diffusion (ID) contribution to spin echo decay, which represents an efficient method for the determination of the concentration of paramagnetic centers without relying on complex and less accurate quantitative EPR procedures, if other pulse length-dependent contributions to relaxation can be neglected. The comparison between the N_{Si} signal in natural

_____

*marco.fanciulli@unimib.it

Si (^{nat}Si) and in isotopically enriched ^{28}Si is fundamental for the interpretation of the origin of the EPR linewidth.

II. EXPERIMENTAL PROCEDURES

The ^{nat}Si samples were prepared using single crystal float zone (100) silicon wafers, with resistivity in the range 1000–5000 Ω cm. The samples, tilted by 7°, were implanted with ^{14}N$^+$ with an energy of 190 keV and a fluence of 5×10^{15} cm^{-2}. Pulsed laser annealing (PLA) has been performed after ion implantation to activate the substitutional paramagnetic centers. The Si samples were exposed in air using pulses from a Nd:YAG laser converted to second harmonic (wavelength of 0.53 μm) [29] and delivering 40-ps pulses with 20-mJ laser energy per shot. The laser was focused with lens characterized by focal distance $f = 9$ cm, but the target was displaced with respect to the focal plane in order to provide a spot diameter of 1 mm. In this way, the typical laser fluence on target was about 2.5 J/cm^2, which is comparable to what previously reported in the literature for efficient laser annealing [26,30,31]. Subsequent shots in different positions were then taken in order to irradiate the whole sample in an approximately uniform way. ^{28}Si samples consisted in a 10 μm ^{28}Si P-doped epilayer grown on top of a standard p-type natural (100) silicon wafer with nominal resistivity 17.5 Ω cm. The dopant concentration in the epilayer is 4.1×10^{16} cm^{-3} and its ^{29}Si residual fraction amounts to less than 0.1%, as reported elsewhere [6]. The ^{28}Si sample underwent ^{14}N$^+$ ion implantation with identical parameters and PLA treatment by a ruby laser in a setup prepared to deliver an analogous laser fluence (approximately 2.2 J/cm^2), yielding a N$_{Si}$ and P$_{Si}$ co-doped system.

Continuous-wave and pulsed EPR investigations were performed in X band with a Bruker Elexsys E580 system equipped with a continuous-flow cryostat. The magnetic field was monitored with a teslameter and calibrated either with DPPH (α,α'-diphenyl-β-picryl hydrazyl) or with BDPA (α,γ-bisdiphenylene-β-phenylallyl) standards, characterized by $g = 2.0036 \pm 0.0003$ and 2.00254 ± 0.00003, respectively [32]. Care was taken in avoiding saturation of continuous-wave EPR signals, and all EPR investigations were performed in dark conditions to exclude effects of light on the spectrum. The instantaneous diffusion investigations were taken through standard echo decay pulse sequences, performed at different pulse power to vary the second pulse turning angle. The pulse lengths were tuned at the applied pulse power by transient nutation experiments, their values being generally fixed to 16 ns for the $\pi/2$ pulse, to allow full single line irradiation. Unless otherwise specified, the echo decay measurements were taken on the lowest-field line, to keep the experiments unaffected by the additional spurious signal observed around $g \sim 2.0057$ (Sec. III A).

III. RESULTS AND DISCUSSION

A. SL5 center

Substitutional nitrogen in silicon has been predicted to introduce a deep level at $\sim$336 meV below the bottom of the conduction band [33]. After an initial controversy, the fundamental state has been recognized as nondegenerate,

similarly to the common shallow donors in silicon [20–24,34]. However, the di-interstitial nitrogen pair was found the most stable N-based point defect making difficult to achieve a high concentration of N$_{Si}$. The as-implanted samples, as well as those treated by furnace or rapid thermal annealing up to 1050 °C, did not reveal any room temperature EPR signal related to N. Only after laser annealing the signal related to N$_{Si}$ could be detected. A comparison between time of flight secondary ion mass spectrometry (ToF-SIMS) data [36], obtained on twin samples, and the N$_{Si}$ concentration, determined by pulsed EPR [28], allowed an estimate of the laser efficiency in activating the substitutional nitrogen centers. This value was found to be $\sim$2.5%, in agreement with previously reported data for similar ion implantation and PLA conditions [25–27].

The EPR spectrum features and the electron spin relaxation times depend on the concentration, as outlined, for example, in Refs. [37] and [38]. Because of the difficult preparation of substitutional nitrogen in silicon, a precise measurement of the N$_{Si}$ concentration profile is not trivial. However, the shape of the EPR spectrum allows to infer that the investigated system is well below the exchange narrowing region. The observation of the ID mechanism in promoting decoherence allows to extract an effective substitutional nitrogen concentration [7,39,40] of $(1.2 \pm 0.2) \times 10^{18}$ cm^{-3} in the case of ^{nat}Si and $(1.3 \pm 0.2) \times 10^{18}$ cm^{-3} for ^{28}Si. These values are far beyond nitrogen solubility in bulk silicon at the melting point (4.5×10^{15} cm^{-3}) and represent roughly the 20% of the solubility in liquid silicon at the melting point (6×10^{18} cm^{-3}) [41–43]. Moreover, the value extracted from ID analysis represents an average over the ensemble of the N$_{Si}$, which contribute to the EPR spectrum and a nonuniform concentration profile centered on this average is expected, as supported by ToF-SIMS profiling [36] assuming that the efficiency of the N$_{Si}$ formation by PLA does not depend on the N local concentration. This result is consistent with the local rapid melting followed by quenching of the silicon surface and subsurface layers induced by pulsed laser annealing [30].

In Fig. 1, continuous-wave EPR spectra of N$_{Si}$ taken with H $\parallel$ [110] at different temperatures are shown along with simulations calculated for the H $\parallel$ [001] and H $\parallel$ [110] directions, while Fig. 2 displays spectra corresponding to H $\parallel$ [111] for the case of ^{28}Si N$_{Si}$.

The observed spectra and their angular dependence, shown in Fig. 3 for ^{28}Si, can be described by a spin Hamiltonian with an anisotropic g-matrix and hyperfine interaction parameters reported in Table I. The investigations on the isotopically enriched spinless ^{28}Si allowed their determination with high accuracy. Efforts were dedicated to the achievement of proper sample alignment, which is critical for such narrow transitions.

The broad line at $g = 2.0057(2)$ is observed also in samples implanted with other species than N and treated with PLA. Upon furnace annealing for 30 minutes at 1000 °C in nitrogen flux both the broad line and the SL5 signal disappear and a new line at g = 2.00260(7) is observed. In amorphous silicon and silicon nitride it is well known that the silicon dangling bond $-Si\equiv Si_3$ ($g \sim 2.006$) shifts to lower g values by increasing the number of N atoms involved reaching the lowest value ($g \sim 2.003$) for $-Si\equiv N_3$ [45,46]. Based on these observations we
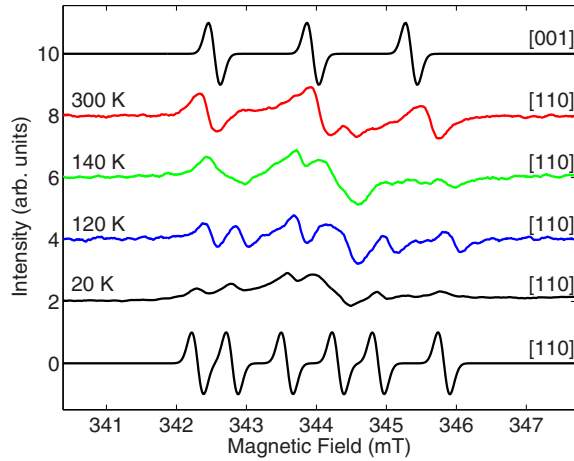
FIG. 1. (Color online) EPR spectra of substitutional nitrogen SL5 center in [nat]Si taken with H ∥ [110] at different temperatures, together with the relative Easyspin simulations [44] of the spectra with H ∥ [110] and H ∥ [001] based on the spin Hamiltonian parameters reported in Table I. At low temperature, a background line at $g \sim 2.0057(2)$ emerges, while at high temperature, the observed spectrum collapses into the three lines observed along the [100] direction due to the motional averaging effect introduced by the defect reorientational dynamics. At room temperature the known increase of the hyperfine splitting is already observable [27]. The magnetic field values were corrected to compare spectra acquired at different spectrometer frequencies.

attribute the broad line to residual post-implantation damage and to silicon microcracks due to the cut of the samples [47] or to direct damage of the Si surface induced by the pulsed laser annealing [30]. Nitrogen may be involved directly in some
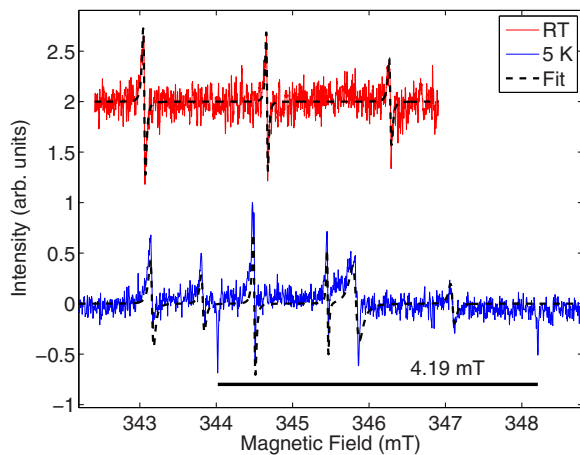

FIG. 2. (Color online) Continuous-wave EPR spectra for [28]Si isotopically enriched N_{Si} taken with H ∥ [111] at 5 K (0.2-μW microwave power) and room temperature spectrum (isotropic, motionally averaged, observed at 630-μW microwave power), along with the corresponding fit. Co-doping is observable in the low-temperature spectrum, where the P doublet (hyperfine splitting = 4.19 mT) is saturated. The low modulation amplitude adopted to avoid overmodulation (5 μT) does not allow to observe the background broad signal. The magnetic field values were corrected to take into account the different spectrometer frequencies.
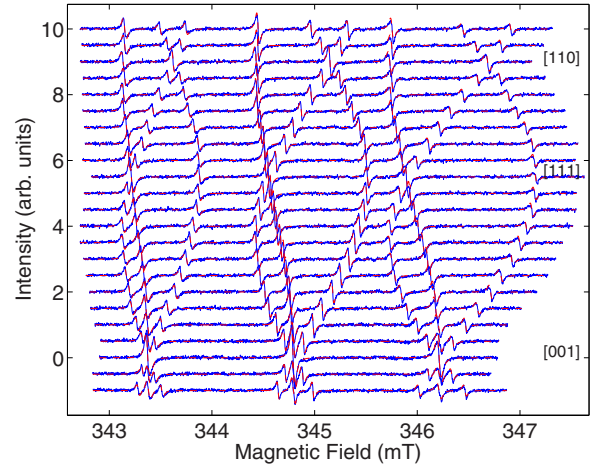

FIG. 3. (Color online) Angular dependence of the EPR spectrum of N_{Si} in [28]Si at 30 K, well below the dynamical transition. Different spectra are stacked by an amount proportional to the orientation angle relative to the [001] direction, and field values are corrected to compare spectra acquired at slightly different working frequencies. Red solid lines represent the best fit. The pattern is fully compatible with the model implying a distortion along the equivalent ⟨111⟩ directions [26].

of these dangling bonds. Upon annealing at 1000 °C only the N-rich dangling bonds survive, as observed by the new line at lower g value. A detailed investigation of the broad line and a firm identification of its nature fall beyond the scope of this article.

The N_{Si} spectrum is essentially determined by the hyperfine splitting of the $S = \frac{1}{2}$ transition with the $I = 1$ spin of ^{14}N atoms. The angular dependence reveals a C_{3v} point symmetry due to a distortion along one of the four equivalent ⟨111⟩ directions. It is known [26] that most of the N_{Si} electron wave function is distributed on the Si atom situated along the distortion direction and to a lesser extent on the ^{14}N atom. This implies also a further hyperfine splitting due to the nearest neighbor [29]Si nuclei ($I = \frac{1}{2}$), which we could not observe in the isotopically enriched [28]Si sample. However, they were observed in the [nat]Si sample and, by keeping constant g factor and hyperfine parameters as extracted from the

TABLE I. Spin Hamiltonian parameters for the N_{Si} center. The principal values of the g and ^{14}N hyperfine matrices are measured using the [28]Si isotopically enriched sample, while [29]Si hyperfine interaction parameters are extracted by measurements using the natural abundance sample. ∥ and ⊥ refer to the ⟨111⟩ directions. For the full width at half maximum, Γ, we report the static value at low temperature for the central transition.

Source	This work		Ref. [26]	
Parameters	∥	⊥	∥	⊥
g	2.00219(4)	2.00847(4)	2.0026(4)	2.0089(4)
A(^{14}N) / MHz	45.85(5)	36.49(4)	45.3(9)	36.3(9)
A([29]Si) / MHz	396.6(2)	234.7(1)	397.5(9)	231.7(9)
Γ ([28]Si)	0.030(2) mT		–	
Γ ([nat]Si)	0.20(2) mT		–	

enriched sample, it was possible to extract also ^{29}Si hyperfine parameters with relatively good precision, as reported also in Table I [48].

We will now focus on the main resonances related to the hyperfine interaction with ^{14}N. At temperatures higher than $\sim$130–150 K, a reorientational dynamics on the time scale of the X-band EPR experiments becomes evident.

At low temperature, signals from the four equivalent crystallographic replicas are observed, but above a certain temperature the thermal energy is sufficient to induce discrete jumps between different configurations of the donor electron wave function, which point to the different $\langle 111 \rangle$ directions. The dynamics induces motional averaging of the spectrum, which collapses to the spectrum observed at low temperature along the [001] direction as outlined in Fig. 1. No quadrupolar contribution was taken into account, nor it was required to reproduce the spectra. A strong quadrupolar contribution would result in a nonzero intensity of forbidden transitions, which should be observable at the sides of the allowed transitions and between them, in the static regime at low temperature.

B. Spectrum thermal evolution

By increasing the temperature across the dynamical transition region, an interesting evolution of the spectrum emerges. We focused on the [111] orientation in the case of ^{nat}Si. The analysis of the data reported in Fig. 4 shows the onset of motional averaging, when the number of observable lines turns from six (three are triply degenerate) to the motionally averaged three, hence a different number of Voigtian components was adopted to best fit the spectra depending on the temperature. The cutoff temperature was 150 K, lower than the literature K-band data (between 150 and 170 K) [26], as
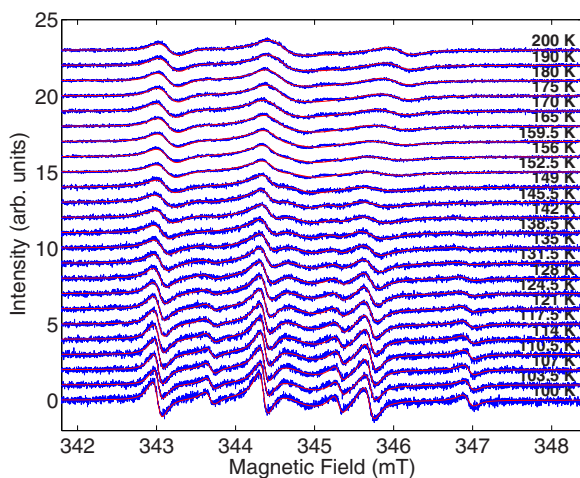

FIG. 5. (Color online) Results of the analysis of data reported in Fig. 4. (a) Evolution of the FWHM Lorentzian Γ_0 (full markers) and Gaussian (empty markers) components of the linewidth of the EPR transitions across the dynamical transition. A model comprising either six (below 150 K) or three (above 150 K) Voigtian components was adopted. A further broad transition due to an extrinsic contribution, already mentioned in the text in Sec. III A, was included in the fitting procedure; (b) temperature trend of the α and β coefficients, which weigh the linewidth dependence on m_I; (c) evolution across the dynamical transition of the hyperfine couplings observed with sample aligned along the [111] direction (the isotropic value is marked by the black dashed line); (d) dynamical correlation times calculated from the Lorentzian linewidth values and from the splitting of two transitions due to different crystallographic branches, along with the relative fit to a temperature-activated behavior (dashed lines). Fitted parameters are reported in Table II. In (a)–(c), the shift from dot to square markers highlights the change in the number of Voigt components.

FIG. 4. (Color online) Temperature evolution of the N_{Si} EPR spectrum taken with $H \parallel [111]$ across the dynamical transition for ^{nat}Si. Data were corrected for the slightly different spectrometer working frequencies adopted at the different temperatures. Each trace is vertically stacked by a constant. Red solid lines represent the best fit with a model of either six ($T < 150$ K) or three ($T > 150$ K) Voigtian components.
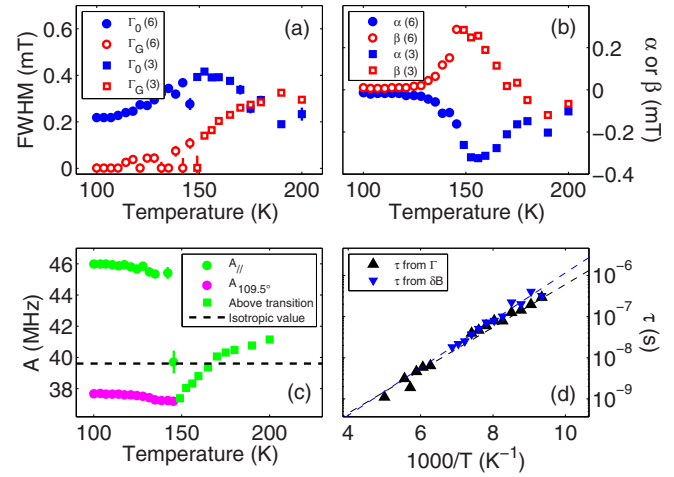
expected, since our X-band spectrometer frequency probes dynamic effects on a longer time scale. The Voigtian width can be expressed in terms of a Gaussian and a Lorentzian full width at half maximum (FWHM), Γ_G and Γ_L, respectively. Since the SL5 center is characterized by g factor and hyperfine interaction anisotropy, Lorentzian width values depend on the nuclear spin quantum number m_I:

$$\Gamma_L = \Gamma_0 + \alpha\, m_I + \beta\, m_I^2,$$

where Γ_0 represents the contribution to the Lorentzian FWHM independent of m_I, also due to broadening mechanisms different from dynamics, whereas α and β are experimental parameters that depend on the details of the reorientational motion, but in general are proportional to the reorientational correlation time and vanish in absence of motion. The temperature dependence of Γ_0, depicted in Fig. 5(a), is clearly affected by the dynamics. At lower temperatures the linewidth is in the slow dynamics regime, manifested by the motional broadening of the two crystallographic replicas along [111] direction, while at higher temperatures the fast dynamics induces a motional narrowing of the Lorentzian component of the merged transitions. The position of the resonances above the dynamical transition is nearer to the field corresponding

TABLE II. Fitting parameters for the thermal activation of the reorientational correlation times reported in Fig. 5(d) along with a comparison to literature data [26]. τ_0 values should be considered as correct within an order of magnitude, due to the reduced number of decades spanned by the dynamical correlation time in our investigations.

Method	ΔE	τ_0
τ from FWHM	100(10) meV	3.7 ps
τ from δB	114(5) meV	2.0 ps
Ref. [26]	110(20) meV	3 ps

to the triply degenerate resonance in the rigid limit, as expected [49].

The fitted values for α and β are comprised in Fig. 5(b). The expression of the width in terms of such parameters was originally derived for dynamic line shape effects in viscous liquids, though it can be demonstrated that the same dependence on m_I holds also for discrete jumps between equivalent configurations in single crystals (like the $\langle 111 \rangle$ orientations in the silicon crystal structure) [50,51]. Across the transition the line shape gradually turns from a Lorentzian to a Voigtian with relevant Gaussian width, as shown in Fig. 5(a), and at the same time $|\alpha|$ and $|\beta|$ increase, while after the transition the decrease of the correlation time makes them tend to zero [Fig. 5(b)] [52–54]. Further theoretical work is required to give a quantitative interpretation of α and β parameters in terms of the correlation time.

Also the hyperfine splitting is temperature dependent. Approaching the transition from lower temperatures it slightly reduces as an effect of motional averaging, while above the transition it slowly increases. In Fig. 5(c), we report the thermal evolution of the hyperfine couplings measured with H ∥ [111]. In the principal axis coordinate system, these are the parallel component $A_\parallel$, and the value $A_{109.5°}$ corresponding to the three remaining [111] directions that form an angle of 109.5° with the former one. Upon heating above 150 K, the hyperfine splitting rapidly reaches the isotropic value, as expected, then continues to increase with a different slope because of the contribution to the dynamics due to the statistically populated on-center configuration with large hyperfine coupling, as derived by high-temperature investigations [27].

Reorientational correlation times can be extracted by following the thermal evolution of the Γ_0 values in the two regimes [26,49,55], and also from the magnetic field separation δB of the transitions which tend to merge [55–58]. Such values are compatible and follow a thermally activated trend $\tau = \tau_0 e^{\frac{\Delta E}{k_B T}}$ as reported in Fig. 5(d). Fitting parameters ΔE and τ_0 are reported in Table II, and agree fairly well with the literature, especially if we consider the relatively small range spanned by τ values in the present investigation. The details of the calculations are reported in Ref. [59].

C. linewidth

As discussed in the previous section, the spectrum observed in the ^{nat}Si:N sample displays a Lorentzian linewidth with full width at half maximum (FWHM) of 0.20(2) mT at 100 K, a temperature sufficiently low to exclude a significant

contribution to the FWHM due to the dynamical transition, but at the same time sufficiently high to avoid complications in the fitting procedures from the central spurious line, which dominates the spectrum at very low temperatures (Fig. 1). Below the dynamical transition the ^{28}Si:N sample displays a strikingly lower Lorentzian linewidth, $\Gamma_0 = 0.030(2)$ mT. Such a narrow width imposes the use of a low modulation amplitude (generally equal to or less than 5 μT and makes the spectrum very sensitive to even slight sample misalignments, which may induce an apparent broadening for overlapped transitions at high symmetry orientations). The modulation frequency of 100 kHz is still sufficiently low to avoid known artifacts [60]. Hence the linewidth was extracted from the fitted value for the crystallographic replica corresponding to the isolated lines for $H \parallel$ [111]. Another remarkable characteristic is that a non-negligible dependence on the nuclear quantum number m_I is observed not only at high temperature, when, in contrast with the case of ^{nat}Si, the line shape remains Lorentzian, but also at low temperatures down to 5 K. The fitted FWHM values for increasing magnetic field line center are 0.050(3), 0.039(2), and 0.054(5) mT at room temperature and 0.070(6), 0.030(2), and 0.088(9) mT at 5 K. These values correspond to $\alpha(5\ K) = -0.009$ mT, $\beta(5\ K) = 0.049$ mT, $\alpha(RT) = -0.002$ mT, $\beta(RT) = 0.013$ mT. The m_I dependence is present independently of the magnetic field scan direction, indicating an intrinsic origin, probably due to the dynamics, rather than a fast passage nuclear polarization effect. In the case of ^{28}Si, the signal-to-noise ratio became worse across the dynamical transition and did not allow to perform a detailed study like in the natural silicon sample.

The picture that emerges from these results indicates that superhyperfine (shf) interactions with ^{29}Si atoms determine the linewidth in the natural-abundance sample, while in the case of the isotopically enriched sample the linewidth is either intrinsic or due to the residual small fraction of ^{29}Si atoms (nominally less than 0.1%). As argued in the following section we attribute the dominant contribution to the linewidth observed in the ^{28}Si enriched sample to dipolar interaction between the N_{Si} centers. However, we shall also point out that, due to the high concentration of N in the implanted region and residual implantation damage, the observed linewidth could be also due to microscopic strains in the volume containing N. To address this subtle issue we have performed micro-Raman spectroscopy investigations on the isotopically enriched sample. These investigations [61–64] allowed to estimate ∼5 μT as an upper limit to the expected strain broadening, a value not negligible, but a factor of six smaller than the observed linewidth.

The FWHM dependence on m_I points out that the fast motion regime determines the linewidth across the dynamical transition, but it has a not negligible effect also at low temperature. Actually, we are not observing a sharp transition that takes place at a well defined temperature, rather it is a dynamical effect described by a temperature-activated correlation time, which allows to describe the system as static or dynamic according to the time scale of the experiment. The fact that this is not observed in the case of ^{nat}Si may be ascribed to the unresolved superhyperfine origin of the line shape, which hides the relatively small effect on the linewidth as compared to the overall broadening. The residual

values for α and β for ^{28}Si at low temperature in fact are much lower than those reported for ^{nat}Si across the transition, and become apparent only thanks to the narrow intrinsic width.

Finally, two issues regarding the ^{nat}Si EPR line shape require further discussion: the Lorentzian shape at low temperatures and the Gaussian component of the Voigtian profile at high temperatures. In the case of shallow V-group donors in ^{nat}Si, the line shape is generally Gaussian, and it is due to an intrinsically narrow Lorentzian line, broadened to a Gaussian by the unresolved superhyperfine interaction with several ^{29}Si coordination shells, probed by the delocalized donor electron wave function [6]. The electron wave function of N_{Si} is more localized than the hydrogenlike donor wave function. This reduces the number of coordination shells available for contributing to the line broadening, by superhyperfine interaction, to such a degree that the Gaussian broadening is not sufficiently intense and the shape remains Lorentzian. A similar modification from Gaussian to partly Lorentzian shape is observed in the spectra of deep defects such as the V$^-$ in silicon by reducing the ^{29}Si fraction [65].

Now we turn to the Gaussian broadening emerging around 150 K. The comparison with the ^{28}Si case confirms that such a broadening is necessarily connected both to the presence of ^{29}Si atoms in the lattice and to the onset of dynamics. We here advance a sort of *dynamical strain broadening* mechanism. The overall picture is the following: as soon as the temperature allows reorientational jumps of the donor electron, not only dynamical effects on the electron interactions start to emerge, but we should expect also small displacements of the Si atoms close to the defect and responsible for the super-hyperfine interactions. The N_{Si} anisotropy implies a local distortion of the lattice, which is strong for the four nearest neighbor silicon atoms but probably extends, though to a lesser degree, also at a larger distance. After each reorientational jump, we may expect a fast reorientation of the electron wave function, which cannot be followed on the same time scale by the neighboring atoms. Hence the lattice is found in an effectively slightly strained configuration, and is likely to start oscillating around the equilibrium configuration as the reorientational jumps take place. From the quantum-mechanical point of view, we may expect that, in the dynamical transition range, suitable local vibrational modes start to be populated and induce a modulation of the superhyperfine interaction at the origin of the linewidth of SL5 center in ^{nat}Si. Each component of the inhomogeneous Lorentzian line in the static regime turns to a distribution of values at the onset of dynamics, yielding the observed Gaussian broadening.

D. Calculation of the dipolar contribution to the linewidth

To understand whether the electron-electron dipolar interaction can be responsible for the observed Γ_0 value, we estimated the dipolar contribution to the linewidth. If we assume a uniform distribution of dopant atoms in a close packed cubic lattice overlapped to the silicon crystal structure with an expanded lattice spacing to take into account the known donor concentration, the theory of moments allows the calculation of the dipolar broadening due to electron-electron dipolar interaction according to the

expression [66]

$$\langle \Gamma_0^2 \rangle = c \frac{3}{4} g^2 \mu_B^2 S(S+1) \sum_j \left(\frac{1 - \cos^2 \theta_{jk}}{r_{jk}^3} \right)^2, \quad (1)$$

where $c = (2\sqrt{2 \ln 2})^2$ is the conversion factor to express the width in FWHM, g and S represent the electron gyromagnetic factor and the electron spin respectively, μ_B is the Boltzmann's constant, θ represents the angle between the external magnetic field and the vector distance which links jth and kth spins, $r_{j,k}$ represents the modulus of their distance, while the k index is fixed on any one of the (equivalent) centers and the j index should in principle run on all electron spins. At the same time, the known concentration allows to calculate an average nearest neighbor distance as

$$\langle r \rangle = \left(\frac{\pi [N]}{6\Omega} \right)^{-1/3},$$

where $[N]$ represents the N_{Si} volume concentration and Ω is the lattice filling factor, which for an fcc lattice equals $\frac{\pi}{3\sqrt{2}}$. By adopting a Lorentz sphere radius sufficiently high to grant convergence (25 Si lattice spacings) and neglecting contributions from the sphere surface or from the external volume, the calculation yields an expected dipolar linewidth (expressed as full width at half maximum, FWHM) of 0.0297 mT, accidentally equal to the experimental value. We further refined such a calculation trying to take into account the concentration profile obtained on twin samples by ToF-SIMS [36] and to avoid at the same time any unjustified assumption on donor placement, which should not, in principle, follow an ordered regular lattice. The procedure consisted in creating a statistically relevant number of configurations ($\sim 10^4$), each around a single donor at a random position, whose depth is generated according to probabilities weighted on ToF-SIMS data. Around each central donor, realistic donor random positions are generated according to the known concentration values at the different depth levels. Configurations implying any couple of donors at nearest neighbor positions were discarded, since they are expected to yield a different paramagnetic center characterized by different spin Hamiltonian parameters. For computational purposes, only a certain volume is considered around the central atom. It has been chosen as a cylinder with basis radius and vertical half-height both of 30 Si lattice spacings. The number of donors created randomly inside the cylinder varies according to the position of the central donor and varies also across the cylinder height, since the SIMS concentration values are sampled with a smaller interval (every ~ 10 lattice spacings in depth). The random donor distribution is then used to calculate the contribution (δ) of the single jth configuration to the overall dipolar broadening, according to the parent expression of Eq. (1) [66]:

$$\langle \Gamma_0^2 \rangle = c \frac{3}{4} g^2 \mu_B^2 S(S+1) \frac{1}{N_D} \sum_j \sum_k \left(\frac{1 - \cos^2 \theta_{jk}}{r_{jk}^3} \right)^2$$

$$= \frac{1}{N_D} \sum_j \delta_j^2, \quad (2)$$

where N_D here is the total number of generated configurations. A histogram of the contributions to the dipolar broadening for
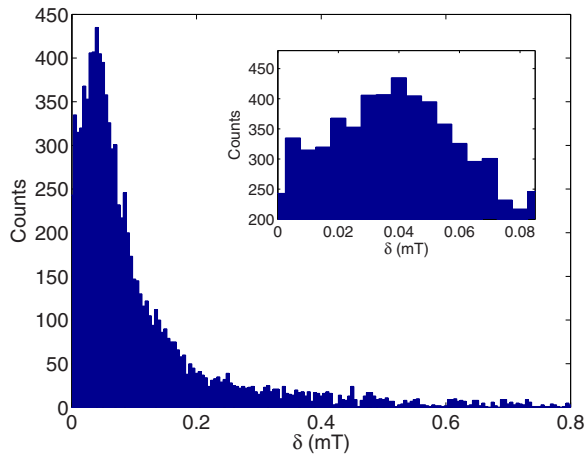
FIG. 6. (Color online) Histogram of the contributions to the dipolar broadening for 10^4 random configurations according to Eq. (2). By considering contributions up to the δ^2 value corresponding to 5% of its maximum statistical frequency count (95% confidence limit) an overall dipolar broadening of 0.038 mT is calculated.

10^4 configurations is reported in Fig. 6. By adopting a cutoff on δ^2 values to within 95% probability confidence around the maximum, we obtain $\langle \Gamma_0^2 \rangle^{\frac{1}{2}} \sim 0.038$ mT, which is in fair agreement with the experimental value. The approximation underlying the whole procedure is that the efficiency of the PLA treatment in activating N on substitutional sites does not depend on the N depth or concentration. Such an assumption appears reasonable for the purposes of the present estimate, but its experimental verification is beyond the scope of the present paper. Hence we attribute the linewidth origin in the static limit for the ^{28}Si sample to the dipolar interaction between the electrons of different substitutional nitrogen centers dispersed in the silicon lattice randomly, but at the same time concurring to the well-defined concentration depth profile revealed by ToF-SIMS [36].

IV. CONCLUSIONS

We have investigated substitutional nitrogen in silicon, a deep donor which should gather in a single physical system several benefits: an almost spinless background of the ^{28}Si nuclei, the possibility to obtain high-purity control and scalability to micro- and nanodevices in current technology and finally an electronic ground state deep in the silicon band gap, which should in principle bring room temperature operation slightly more close to hand. The dynamics of the center, here investigated, may be also exploited for spin manipulation via, for example, external stress. In the present work we focused on the temperature evolution of the spectrum and on the origin of the line shape, comparing the cases of N_{Si} in ^{nat}Si and ^{28}Si samples. We conclude that in the case of natural silicon the linewidth is dominated by unresolved superhyperfine interaction with ^{29}Si atoms dispersed in the lattice. The intrinsic dipolar broadening emerges for ^{28}Si isotopic enrichment, as confirmed also by statistical calculations. Investigations of the spin-spin and spin-lattice relaxation times in the same system will be the topic of a following paper [28].

[1] B. E. Kane, Nature (London) **393**, 133 (1998).

[2] A. M. Tyryshkin, J. J. L. Morton, S. C. Benjamin, A. Ardavan, G. A. D. Briggs, J. W. Ager, and S. A. Lyon, J. Phys.: Condens. Matter **18**, S783 (2006).

[3] D. Loss and D. P. DiVincenzo, Phys. Rev. A **57**, 120 (1998).

[4] D. P. DiVincenzo, Fortschr. Phys. **48**, 771 (2000).

[5] A. Debernardi, A. Baldereschi, and M. Fanciulli, Phys. Rev. B **74**, 035202 (2006).

[6] M. Fanciulli, P. Höfer, and A. Ponti, Physica B **340–342**, 895 (2003).

[7] A. Ferretti, M. Fanciulli, A. Ponti, and A. Schweiger, Phys. Rev. B **72**, 235201 (2005).

[8] G. W. Morley, P. Lueders, M. H. Mohammady, S. J. Balian, G. Aeppli, C. W. M. Kay, W. M. Witzel, G. Jeschke, and T. S. Monteiro, Nat. Mater. **12**, 103 (2013).

[9] J. Preskill, Proc. R. Soc. London Ser. A **454**, 385 (1998).

[10] M. Belli, M. Fanciulli, and N. V. Abrosimov, Phys. Rev. B **83**, 235204 (2011).

[11] B. E. Kane, N. S. McAlpine, A. S. Dzurak, R. G. Clark, G. J. Milburn, He Bi Sun, and H. Wiseman, Phys. Rev. B **61**, 2961 (2000).

[12] R. E. George, W. Witzel, H. Riemann, N. V. Abrosimov, N. Nötzel, M. L. W. Thewalt, and J. J. L. Morton, Phys. Rev. Lett. **105**, 067601 (2010).

[13] C. D. Weis, C. C. Lo, V. Lang, A. M. Tyryshkin, R. E. George, K. M. Yu, J. Bokor, S. A. Lyon, J. J. L. Morton, and T. Schenkel, Appl. Phys. Lett. **100**, 172104 (2012).

[14] P. A. Mortemousque, T. Sekiguchi, C. Culan, M. P. Vlasenko, R. G. Elliman, L. S. Vlasenko, and K. M. Itoh, Appl. Phys. Lett. **101**, 082409 (2012).

[15] M. H. Mohammady, G. W. Morley, A. Nazir, and T. S. Monteiro, Phys. Rev. B **85**, 094404 (2012).

[16] S. J. Balian, M. B. A. Kunze, M. H. Mohammady, G. W. Morley, W. M. Witzel, C. W. M. Kay, and T. S. Monteiro, Phys. Rev. B **86**, 104428 (2012).

[17] G. D. Watkins, Semicond. Sci. Tech. **6**, B111 (1991).

[18] C. P. Ewels, R. Jones, S. Öberg, J. Miro, and P. Deák, Phys. Rev. Lett. **77**, 865 (1996).

[19] S. T. Pantelides, W. A. Harrison, and F. Yndurain, Phys. Rev. B **37**, 1016 (1988).

[20] J. P. Goss, I. Hahn, R. Jones, P. R. Briddon, and S. Öberg, Phys. Rev. B **67**, 045206 (2003).

[21] S. J. Sferco and M. C. G. Passeggi, J. Phys. C **18**, 3717 (1985).

[22] G. G. DeLeo, W. B. Fowler, and G. D. Watkins, Phys. Rev. B **29**, 3193 (1984).

[23] J. A. Vergés, J. Phys. C **14**, 365 (1981).

[24] P. A. Schultz and R. P. Messmer, Phys. Rev. B **34**, 2532 (1986).

[25] K. L. Brower, Phys. Rev. Lett. **44**, 1627 (1980).

[26] K. L. Brower, Phys. Rev. B **26**, 6040 (1982).

[27] K. Murakami, H. Kuribayashi, and K. Masuda, Phys. Rev. B **38**, 1589 (1988).

[28] M. Belli and M. Fanciulli (unpublished).

[29] A. Faenov, T. Pikuz, A. Magunov, D. Batani, G. Lucchini, F. Canova, and M. Piselli, Laser Part. Beams **22**, 373 (2004).

[30] K. Murakami, K. Masuda, Y. Aoyagi, and S. Namba, Physica B+C **116**, 564 (1983).

[31] K. Murakami, H. Itoh, K. Takita, and K. Masuda, Appl. Phys. Lett. **45**, 176 (1984).

[32] P. Höfer and Bruker (private communication).

[33] S. T. Pantelides and C. T. Sah, Phys. Rev. B **10**, 638 (1974).

[34] A. K. Ramdas and S. Rodriguez, Rep. Prog. Phys. **44**, 1297 (1981).

[35] See Supplemental Material at http://link.aps.org/supplemental/10.1103/PhysRevB.89.115207 for ToF-SIMS investigations (Section S2).

[36] See Ref. [35], Sec. S2, for ToF-SIMS investigations.

[37] G. Feher, Phys. Rev. **114**, 1219 (1959).

[38] G. Feher and E. A. Gere, Phys. Rev. **114**, 1245 (1959).

[39] S. S. Eaton and G. R. Eaton, J. Magn. Reson., Ser. A **102**, 354 (1993).

[40] See Ref. [35], Sec. S7, for details on the calculation of the donor concentration from instantaneous diffusion investigations.

[41] Y. Yatsurugi, N. Akiyama, Y. Endo, and T. Nozaki, J. Electrochem. Soc. **120**, 975 (1973).

[42] T. Nozaki, Y. Yatsurugi, N. Akiyama, Y. Endo, and Y. Makide, J. Radioanal. Chem. **19**, 109 (1974).

[43] J. B. Mitchell, J. Shewchun, D. A. Thompson, and J. A. Davies, J. Appl. Phys. **46**, 335 (1975).

[44] S. Stoll and A. Schweiger, J. Magn. Reson. **178**, 42 (2006).

[45] T. Wang, L. Zhang, X. Fan, J. Hu, and J. Mo, J. Appl. Phys. **74**, 6313 (1993).

[46] A. Stesmans and G. Van Gorp, Phys. Rev. B. **52**, 8904 (1995).

[47] A. Hobbs, R. C. Barklie, P. L. F. Hemment, and K. Reeson, J. Phys. C **19**, 6433 (1986).

[48] See Ref. [35], Secs. S3–S5, for details on the fitting of the spectra with Voigtian components and on the fitting of the angular variation of transition field values.

[49] G. D. Watkins and J. W. Corbett, Phys. Rev. **134**, A1359 (1964).

[50] Z. Zimpel, Physica B+C **145**, 311 (1987).

[51] Z. Zimpel, J. Magn. Reson. **85**, 314 (1989).

[52] J. A. Weil, J. R. Bolton, and J. E. Wertz, *Electron Paramagnetic Resonance: Elementary Theory and Practical Applications* (John Wiley & Sons, New York, 1994).

[53] C. P. Poole, Jr., *Electron Spin Resonance: A Comprehensive Treatise on Experimental Techniques* (John Wiley & Sons, New York, 1983).

[54] D. Kivelson, J. Chem. Phys. **33**, 1094 (1960).

[55] H. S. Gutowsky and A. Saika, J. Chem. Phys. **21**, 1688 (1953).

[56] M. Fanciulli, S. Jin, and T. D. Moustakas, Physica B **229**, 27 (1996).

[57] H. S. Gutowsky and G. E. Pake, J. Chem. Phys. **18**, 162 (1950).

[58] N. Bloembergen, E. M. Purcell, and R. V. Pound, Phys. Rev. **73**, 679 (1948).

[59] See Ref. [35], Sec. S6, for details on the extraction of parameters describing the dynamics of the investigated system.

[60] G. R. Eaton, S. S. Eaton, D. P. Barr, and R. T. Weber, *Quantitative EPR* (SpringerWien, New York, 2010).

[61] See Ref. [35], Sec. S8, for details on the estimate of the *g*-strain broadening induced by implantation.

[62] I. De Wolf, Semicond. Sci. Technol. **11**, 139 (1996).

[63] E. Bonera, M. Fanciulli, and D. N. Batchelder, J. App. Phys. **94**, 2729 (2003).

[64] D. K. Wilson and G. Feher, Phys. Rev. **124**, 1068 (1961).

[65] D. V. Guseinov, A. A. Ezhevskii, and C. A. J. Ammerlaan, Physica B **381**, 164 (2006).

[66] C. P. Slichter, *Principles of Magnetic Resonance*, Springer Series in Solid-State Science, 3rd ed. (Springer-Verlag, Berlin, 1990), reprinted in 1996.